Magnetism in doped infinite-layer $NdNiO_2$ studied by combined density functional theory and dynamical mean-field theory

Dachuan Chen,[1,2,*] Peiheng Jiang,[1,*] Liang Si,[1,3,4] Yi Lu,[5,6,†] and Zhicheng Zhong[1,7,‡]

[1]*CAS Key Laboratory of Magnetic Materials and Devices & Zhejiang Province Key Laboratory of Magnetic Materials and Application Technology, Ningbo Institute of Materials Technology and Engineering, Chinese Academy of Sciences, Ningbo 315201, China*

[2]*College of Materials Science and Opto-Electronic Technology, University of Chinese Academy of Sciences, Beijing 100049, China*

[3]*School of Physics, Northwest University, Xi'an 710069, China*

[4]*Institute for Solid State Physics, Vienna University of Technology, 1040 Vienna, Austria*

[5]*National Laboratory of Solid State Microstructures and Department of Physics, Nanjing University, Nanjing 210093, China*

[6]*Collaborative Innovation Center of Advanced Microstructures, Nanjing University, Nanjing 210093, China*

[7]*China Center of Materials Science and Optoelectronics Engineering, University of Chinese Academy of Sciences, Beijing 100049, China*

(Received 27 December 2021; revised 17 June 2022; accepted 23 June 2022; published 6 July 2022)

The recent observation of superconductivity in infinite-layer nickelates has brought intense debate on the established knowledge of unconventional superconductivity based on the cuprates. Despite many similarities, the nickelates differ from the cuprates in many characteristics, the most notable of which is the magnetism. Instead of a canonical antiferromagnetic (AFM) Mott insulator as the undoped cuprates, from which the superconductivity is generally believed to arise upon doping, the undoped nickelates show no sign of magnetic ordering in experiments. Through a combined density functional theory, dynamical mean-field theory, and model study, we show that although the increased energy splitting between O-p orbital and Cu/Ni-d orbital (Δ_{dp}) results in a larger magnetic moment in nickelates, it also leads to stronger AFM/ferromagnetism competition and weaker magnetic exchange coupling. Meanwhile, the self-doping effect caused by Nd-d orbital screens the magnetic moment of Ni. The Janus-faced effect of Δ_{dp} and self-doping effect together give a systematic understanding of magnetic behavior in nickelates and explain recent experimental observations.

DOI: 10.1103/PhysRevB.106.045105

I. INTRODUCTION

Since the discovery of high-temperature superconductivity (HTSC) in cuprates [1], enormous efforts have been devoted to understanding its microscopic mechanism and searching for new materials hosting HTSC [2–4]. The quasi-two-dimensional CuO_2 planes in cuprates are generally regarded as a key element in realizing HTSC, whose antiferromagnetic (AFM) Mott insulating phase quickly melts away upon hole doping, following which the HTSC emerges [4,5]. As the cuprates fall into the charge-transfer insulator category [6], the doped holes primarily reside on the O sites, which resonate around a Cu site, and their spins combine with the spin on Cu into a singlet [7]. These Zhang-Rice singlets move around the lattice and form an effective one-band model, which serves as the starting point of many theoretical studies of HTSC [4]. With this general picture in mind, it is then natural to ask if the isoelectronic infinite-layer nickelates $ANiO_2$ with similar structural building blocks are also superconducting [8].

This question has been answered recently by the discovery of superconductivity in hole-doped $Nd_{0.85}Sr_{0.15}NiO_2$ with $T_c \sim 15$ K by Li *et. al.* [9,10] and confirmed later by several other groups [11–13]. Despite the great similarities between the nickelates and the cuprates, stark differences remain, especially in their magnetic properties, which raise questions regarding the validity of a uniformed description of their superconductivity. Neutron diffraction studies show that the magnetic moment of cuprates is about 0.5 μ_B [14]. However, based on the hypothetical G-type AFM structure, neutron diffraction experiments indicate that the magnetic moment of nickelates (0.05 μ_B/Ni [8] or 0.06 μ_B/Ni [15]) is much smaller than that of cuprates. While several first-principles studies propose that the AFM order is the ground state in nickelates [16–27], experiments have so far failed to obtain direct evidence of long-range magnetic order in them [8,15].

On the other hand, short-range AFM interactions are observed in NMR [28], Raman spectroscopy [29], and resonant inelastic x-ray scattering [30,31] experiments. Such a magnetic behavior is also reported by plenty of theoretical studies [25–27,32,33], some of which further suggest that the exchange interaction of nickelates is not stronger than that of cuprates [25,26].

In this paper, we focus on the origin of the magnetic differences between the cuprates and the nickelates and perform a systematic study on their magnetic properties with both density functional theory plus Hubbard U (DFT + U) and dynamical mean-field theory (DMFT). Our calculations show several important consequences of the large Δ_{dp} and self-doping effect in nickelates. First, the energy difference

*These authors contributed equally to this work.
†Corresponding author: yilu@nju.edu.cn.
‡Corresponding author: zhong@nimte.ac.cn.

between various magnetic orders is quite small in undoped nickelates, leading to the competition of different magnetic orders and even possible spin fluctuation [34,35]. Second, while the AFM state is energetically more favorable in undoped and electron doped nickelates, an intralayer ferromagnetic (FM) state is surprisingly stabilized upon hole doping. Third, we found that the magnetic moment of Ni is larger than that of Cu. The last observation is reconciled with the seemingly contradicting experimental results by further considering the self-doping and dynamic screening effects in nickelates using DMFT. In addition, our exact diagonalization (ED) calculation of small clusters reports a smaller magnetic exchange interaction J in nickelates, which is still comparable to that in the cuprates.

II. METHODS

A. DFT

We performed DFT calculations within the generalized gradient approximation Perdew-Burke-Ernzerhof (PBE) functional and the projector augmented wave (PAW) method as implemented in the Vienna *ab initio* simulation package (VASP) [36–38] and WIEN2K [39]. In addition to $NdNiO_2$, the isostructural $CaCuO_2$ studied for comparison. The Nd-4f orbitals are treated as core states. The relaxed lattice constants are $a = b = 3.88$ Å and $c = 3.35$ Å for $NdNiO_2$ and $a = b = 3.81$ Å and $c = 3.17$ Å for $CaCuO_2$. The strain effect, which is discussed in Appendix A, does not affect the conclusions of this work. Electronic correlations on Ni/Cu-3d and Nd-5d are included by the DFT + U method with $U = 5.0$ and 2.0 eV, respectively. We also adopted the Heyd-Scuseria-Ernzerhof (HSE06) hybrid functional for calculations, because this functional performs exceptionally well in describing systems with a mixture of itinerant and localized electrons from different orbitals [40]. The strongly constrained and appropriately normed (SCAN) functional which enables improved predictions for oxides [41] is also included in calculations. To determine the magnetic ground state, various possible magnetic orders are considered. Since the interlayer interactions are weaker than the intralayer ones, here we mainly focus on intralayer magnetic order, including FM (0,0,0), C-type AFM $(\pi, \pi, 0)$ ($\sqrt{2} \times \sqrt{2} \times 1$ supercell), and stripy AFM $(\pi, 0, 0)$ (S-type, $2 \times 2 \times 1$ supercell). Some other complex orders are also carefully checked (see Appendix B). The kinetic energy cutoff is set to 500 eV. The Brillouin zone is sampled with $13 \times 13 \times 15$, $8 \times 8 \times 12$ and $8 \times 8 \times 8$ Monkhorst-Pack **k** grids for PBE calculations of unit cell and supercell and HSE06 (see Appendix C) calculations, respectively. The doping is simulated by using virtual crystal approximation (VCA). We also calculated Sr doping by constructing a supercell of $NdNiO_2$, which shows similar results with the VCA scheme.

B. ED

To obtain the exchange interaction J, we construct a three-band Hubbard model in a Cu_5O_{16} cluster relative to a Cu-d^{10}, O-p^6 vacuum state, and map the low-energy spectrum to that of a Heisenberg model. For simplicity, the Coulomb interaction parameters are kept the same for both the nickelate and the cuprate with values listed in Ref. [42]. The calculation is performed using QUANTY [43].

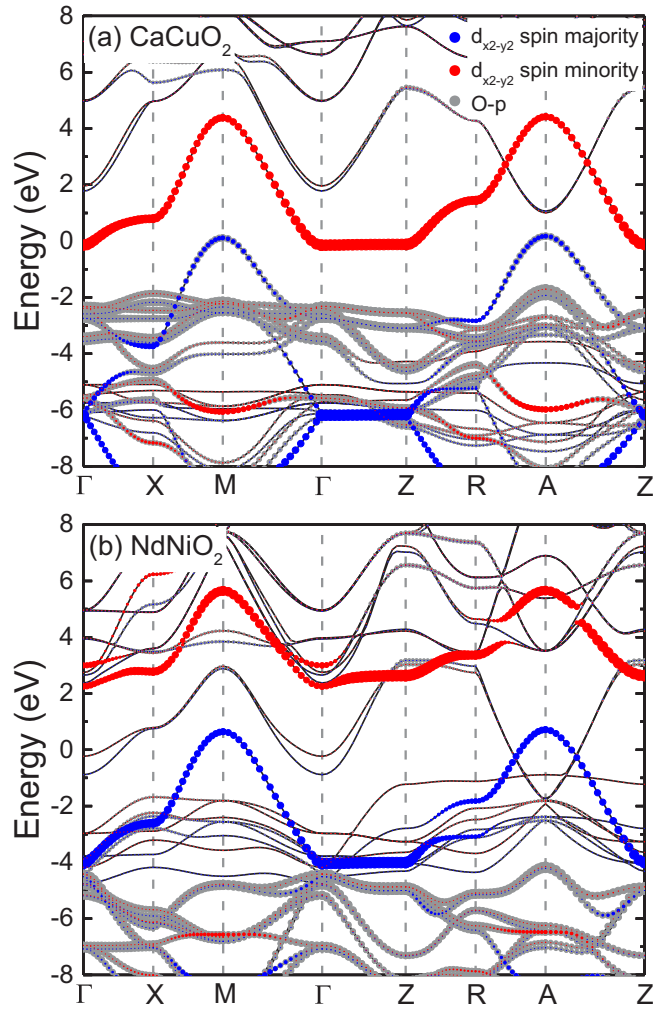

FIG. 1. Electronic band structures of (a) $CaCuO_2$ and (b) $NdNiO_2$ with FM order calculated by HSE hybrid functional.

C. DMFT

For the DMFT calculations, the DFT band structure around the Fermi level is projected onto Wannier functions [44,45] using WIEN2WANNIER [46,47] and supplemented by a local density-density interaction. To study the magnetic properties of $NdNiO_2$ with and without self-doping effect, we choose Ni-d orbitals as the correlated space to calculate the magnetic phase diagram and conductivity. The self-doping effect is then included by modifying electron fillings on the DMFT level. To study the local screening effect from Nd, we also construct a Nd-d + Ni-d model with 10 bands. The interaction parameters are computed by constrained random-phase approximation [48–50], which gives an averaged interorbital interaction $U' = 3.10$ eV and Hund's exchange $J = 0.65$ eV for Ni. The intraorbital Hubbard interaction follows as $U = U' + 2J$. The resulting Hamiltonian is then solved in DMFT using continuous-time quantum Monte Carlo simulations in the hybridization expansions [51] implemented in

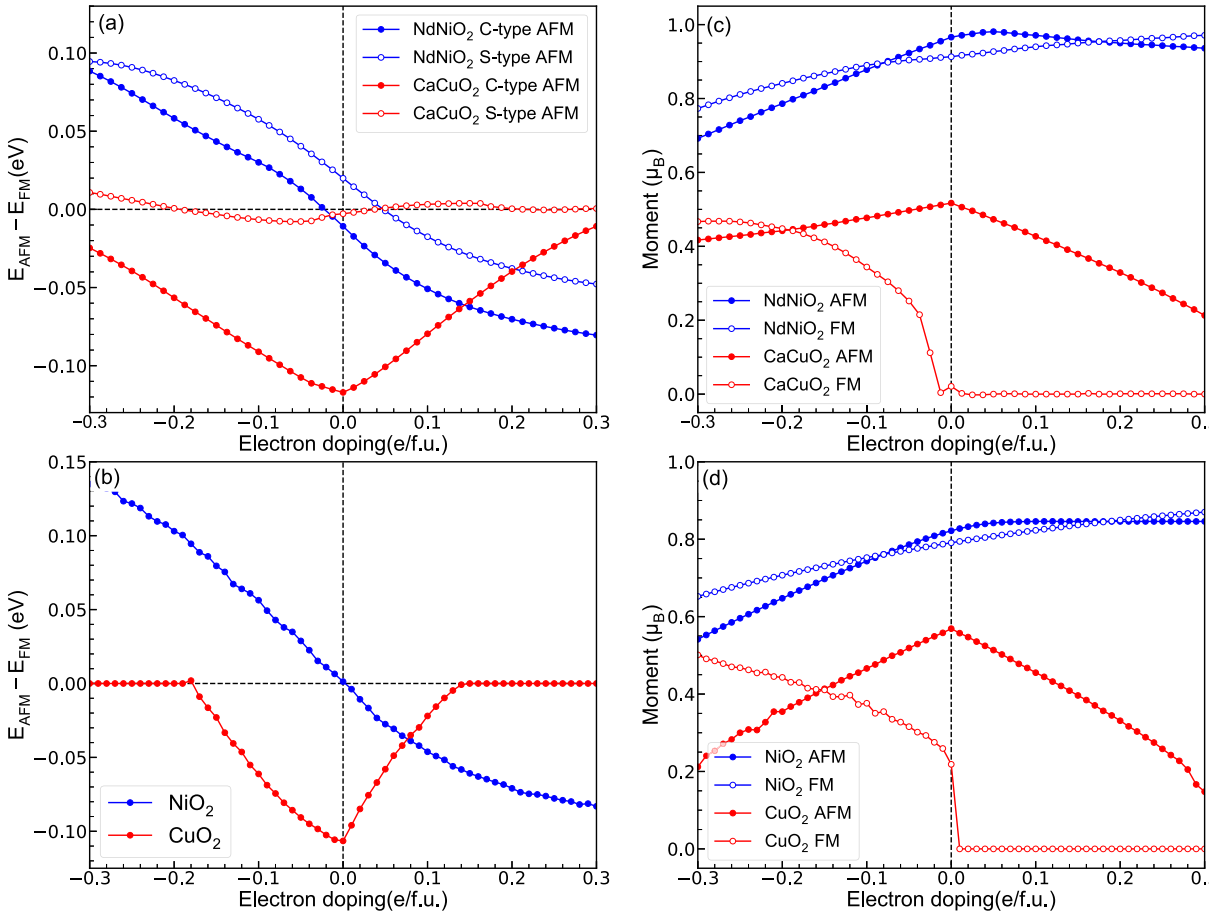

FIG. 2. [(a), (b)] Total energy difference between AFM and FM magnetic orders at different doping concentrations with (a) DFT calculations and (b) mean-field solutions. The electron and hole doping are represented by positive and negative doped electrons, respectively. The energy of FM order is set to zero. [(c), (d)] Magnetic moment of $NdNiO_2$ and $CaCuO_2$ at different doping concentrations with (c) DFT calculations and (d) mean-field solutions.

w2dynamic [52,53]. The maximum entropy method [54,55] is employed for analytic continuation of the spectra.

III. RESULTS AND DISCUSSIONS

A. DFT calculations

The HSE calculated electronic band structures of $CaCuO_2$ and $NdNiO_2$ with FM configuration are shown in Fig. 1. We first focus on the spin splitting of Cu/Ni-d orbital and find that the splitting of $NdNiO_2$ is noticeably larger than $CaCuO_2$. Especially for the $d_{x^2-y^2}$ orbital near Fermi level, the spin splitting of $NdNiO_2$ is 0.74 eV larger than $CaCuO_2$ at M point (5.01 eV for $NdNiO_2$ and 4.27 eV for $CaCuO_2$). This indicates a larger local moment of Ni than that of Cu. Indeed, the projected moment is 0.94 μ_B for Ni in $NdNiO_2$ and 0.72 μ_B for Cu in $CaCuO_2$. We also calculate the electronic band structure and moment of $CaCuO_2$ and $NdNiO_2$ with PBE + U and SCAN functional; both give similar results. The larger magnetic moment of $NdNiO_2$ can be explained by the suppressed moment screening, which is determined by the energy splitting between Ni/Cu-$d_{x^2-y^2}$ and O-p orbitals (Δ_{dp}). A large (small) Δ_{dp} indicates a weak (strong) hybridization between O-p and Ni/Cu-$d_{x^2-y^2}$ orbitals and hence a weak(strong) screening and a large (small) magnetic moment. The calculated Δ_{dp} of $NdNiO_2$ is 2∼3 eV larger than that of $CaCuO_2$, whose exact value also depends on calculation method and detail [56,57]. Based on the calculations, we find that the larger spin splitting and Δ_{dp} contribute to a larger local moment in nickelate than in cuprate, so that the pristine nickelate is not nonmagnetic (NM).

In addition to the large local moment, another key factor for generating long-range magnetic order is magnetic interaction. Without strong magnetic interaction, the system will converge to a NM state. To investigate the interaction, we further calculate various magnetic orders and their doping dependence in both the nickelate and the cuprate. Figure 2(a) shows the DFT + U calculated energy difference between various magnetic orders upon electron/hole doping. For $CaCuO_2$, the ground state is in a stable C-type AFM state for the undoped case. When electron and hole doping concentrations increase from 0 to 0.3 /f.u., the energy difference between C-type AFM and FM (the DFT + U calculated FM order converges to NM order with $U_{Cu} = 5$ eV when the doping concentration is larger than 0.01 e/f.u.) decreases from 120 to 25 meV for hole doping and 11 meV for electron doping. This result indicates that both electron and hole doping can suppress AFM coupling of $CaCuO_2$, leading to the disappearance of long-range magnetic order. For the undoped $NdNiO_2$, the energy

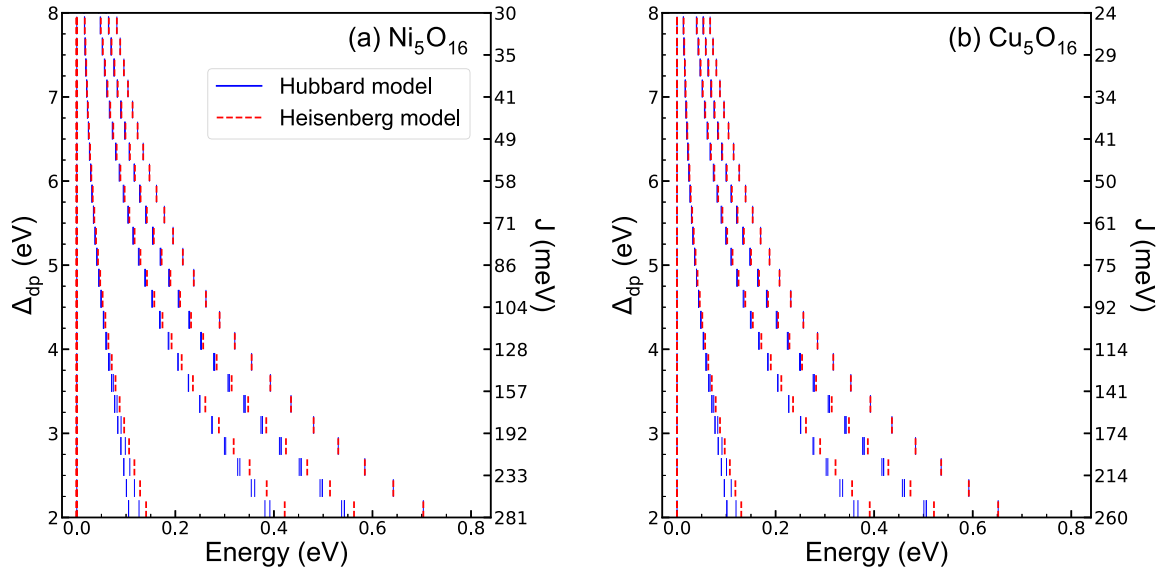

FIG. 3. The low-energy spectrum for Cu_5O_{16} and Ni_5O_{16} clusters calculated in the three-band Hubbard model (blue line) in comparison with mappings onto effective Heisenberg model (red dash line) for half filled case.

difference between AFM and FM orders is −11 meV for C-type AFM and 25 meV for S-type AFM; such a small energy difference implies that a competition exists between these magnetic orders. With electron doping larger than 0.02 /f.u., the C-type AFM state has the lowest energy, which is about 30 or 80 meV lower than S-type AFM or FM state, respectively. In the case of hole doping, a striking intralayer FM state can be induced in $NdNiO_2$, which becomes more stable when the hole doping concentration increases. With 0.3 /f.u. hole doping, the energy of FM can be 90 meV lower than that of AFM. We note that signs of FM order have also been observed experimentally in overdoped cuprates [58,59].

The DFT + U calculated local magnetic moment of doped $NdNiO_2$ and $CaCuO_2$ are shown in Fig. 2(c). For $CaCuO_2$, the moment maximizes at half filling with a value of 0.5 μ_B and gradually decreases with increasing electron or hole doping. For $NdNiO_2$, due to the self-doping effect induced by Nd-d orbitals, the maximal moment appears after slight electron doping. For both hole and electron doping, the moments of $NdNiO_2$ are always larger than $CaCuO_2$, which is consistent with the large spin splitting in nickelate and is contributed by self-doping effect and large energy-gap Δ_{dp} as discussed above. To check the reliability of these results, we also perform HSE calculations which give similar conclusions with the DFT + U scheme.

Our DFT calculated result is in agreement with the well-known fact that the undoped cuprate is a Mott insulator. Its ground state is intralayer AFM, and this long-range magnetic order is well established by Cu-O-Cu superexchange interaction. Doping can suppress the AFM order and close the gap and then drive the pseudogap and finally the superconducting phase. For nickelate, the large Δ_{dp} reduces the Ni-O-Ni superexchange interaction and weakens the AFM order. Moreover, the self-doping effect

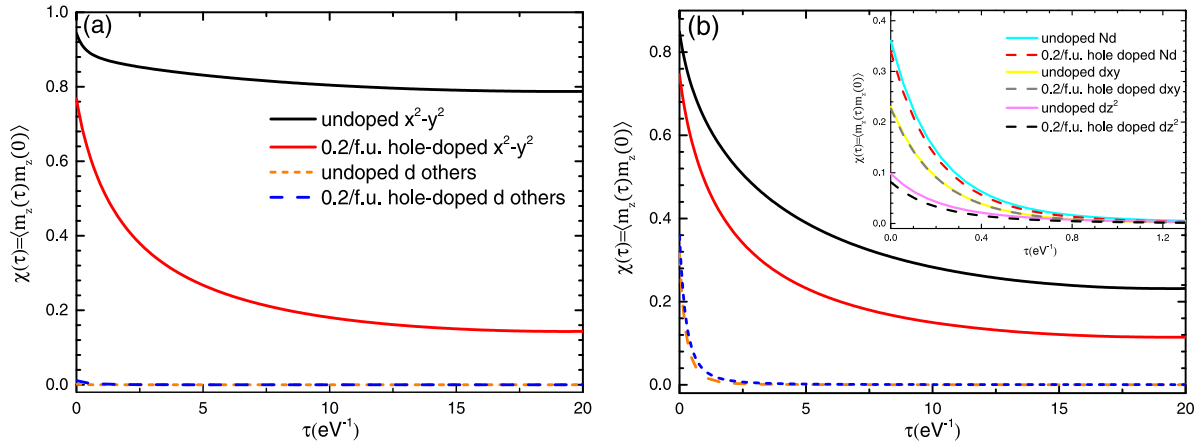

FIG. 4. Orbital-resolved local spin-correlation functions $\chi(\tau) = \langle \hat{m}_z(\tau)\hat{m}_z(0)\rangle$ calculated by DMFT at $T = 300$ K in the Kanamori form, $\beta/2 \approx 19.34\,\mathrm{eV}^{-1}$. (a) Ni-$d$-only model, (b) Nd-$d$ + Ni-d model; inset: The contributions of Nd atom. The black curve in (b) shows a reduction compared with that in (a) due to the self-doping effect.

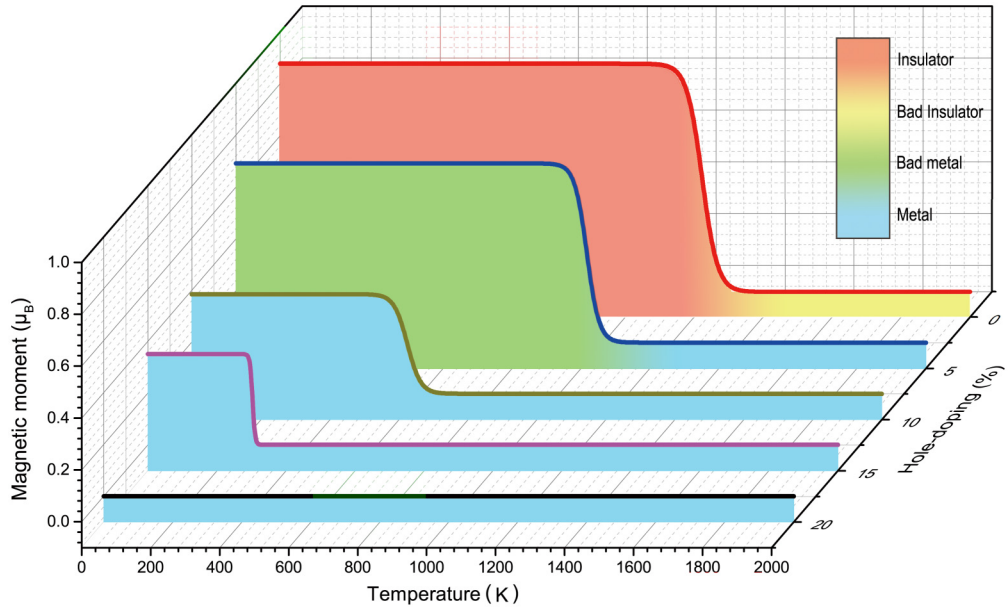

FIG. 5. Phase diagram of $NdNiO_2$ calculated by two-site Ni-d-only DMFT method, which shows the magnetic moment and conductivity at different temperature and hole doping concentration. The black, gray, mazarine, and blue circle represent AFM insulator, AFM metal, PM insulator, and PM metal, respectively. The phases of bad insulator and bad metals are defined by Ref. [64].

contributes a large kinetic part and then results in a metallic state which favors spin parallel. Therefore both of these two effects drive $NdNiO_2$ to be in a competing magnetic phase.

B. Mean-field solution of the Emery model

To further confirm that the magnetic difference between nickelate and cuprate mainly comes from Δ_{dp} and the doping effect, we construct a minimal three-orbital Hubbard model on the two-dimensional CuO_2/NiO_2 plane that captures the relevant physical degrees of freedom,

$$\mathcal{H} = t_{dp}\sum_{<ij>\sigma} d^{\dagger}_{i\sigma}p_{j\sigma} + t_{pp}\sum_{<ij>\sigma} p^{\dagger}_{i\sigma}p_{j\sigma} + t_{dd}\sum_{<ij>\sigma} d^{\dagger}_{i\sigma}d_{j\sigma} + \Delta_{dp}\sum_{i\sigma} p^{\dagger}_{i\sigma}p_{i\sigma} + U_d\sum_{i} n^{\uparrow}_{di}n^{\downarrow}_{di}, \quad (1)$$

where $d^{\dagger}_{i\sigma}$ and $p^{\dagger}_{i\sigma}$ are creating operators of spin $\sigma(\uparrow,\downarrow)$ at the i-th site of $d_{x^2-y^2}$ and $p_{x/y}$ orbitals, respectively. For simplicity, we include Coulomb interaction only for the $d_{x^2-y^2}$ orbital. The hopping parameters t_{dp}, t_{pp}, t_{dd}, and Δ_{dp} are taken from Ref. [57]. For cuprate, $t_{dp} = 1.48\,\text{eV}$, $t_{pp} = 0.91\,\text{eV}$, $t_{dd} = 0.15\,\text{eV}$, and $\Delta_{dp} = 0.95\,\text{eV}$, while for nickelate, we only change Δ_{dp} to 4.45 eV. Because the local interaction of Ni-d orbital is similar with Cu-d, we use the Hubbard interaction $U_d^{Ni} = U_d^{Cu} = 4\,\text{eV}$ (note that to be consistent with DFT calculations and take into account the overestimation of polarization in mean-field solution, we set a relatively small Hubbard U). The Nd-d band is excluded in the calculation to minimize the number of parameters in the model. To account for its self-doping effect, the zero-doping reference point is shifted by 0.15 hole/f.u. according to the DFT calculation [60].

For comparison, we calculate the total energy and magnetic moment of CuO_2/NiO_2 planes with different electron concentrations within the Hartree-Fock mean-field approximation. Figure 2(b) shows the energy difference of the AFM and FM states ($E_{\text{AFM}} - E_{\text{FM}}$). The value of energy difference is set to zero when the ground state is paramagnetic (PM). For cuprate, since the Δ_{dp} in cuprate is small, the adjacent spins on Cu atom show strong AFM coupling through the superexchange interaction, which is proportionate to $1/\Delta_{dp}^2$. The relatively large superexchange coupling leads to AFM order when undoped. As for nickelate, the AFM coupling is weakened due to the larger Δ_{dp}. The kinetic energy of the extra holes in the undoped nickelate further frustrate the AFM order. Based on this mechanism, nickelate and cuprate exhibit completely different behaviors in their ground states. Cuprate shows a stable AFM in the parent compound, and it is suppressed upon doping, while nickelate shows a FM and AFM competition phase when the hole concentration increases. These complicated magnetic competition phases, such as spin spirals, nematicity and FM domain walls, have been discussed on the mean-field level [61]. Especially with hole doping, both DFT calculations and model analysis give the same intralayer FM ground-state configuration. Please note that both DFT and model analysis are on the mean-field level, which always overestimate magnetic order. For the effect of Nd-d orbitals, the self-doping effect is well known; actually, some groups suggest that the hybridization effect is also important [62], which may induce Kondo context [63] and/or may contribute to RKKY coupling between Ni moments as suggested by a recent experiment [31].

Figure 2(d) shows the calculated magnetic moment. The key difference between cuprate and nickelate is the larger Δ_{dp} and the self-doping effect in nickelate. The large Δ_{dp} in nickelate induces strong spin polarization in d orbital and thus a larger local moment. In cuprate, the strong d-p hybridization

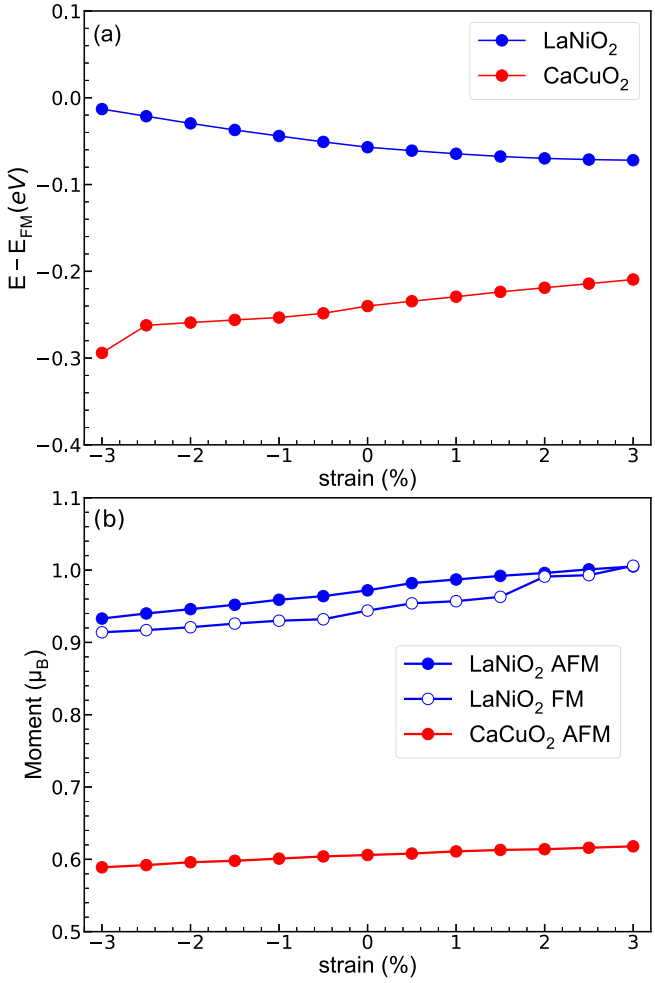

FIG. 6. HSE calculations of $LaNiO_2$ and $CaCuO_2$ at different strains. (a) The energy difference between G-type AFM and FM. (b) The local moment of Ni and Cu for G-type AFM and FM.

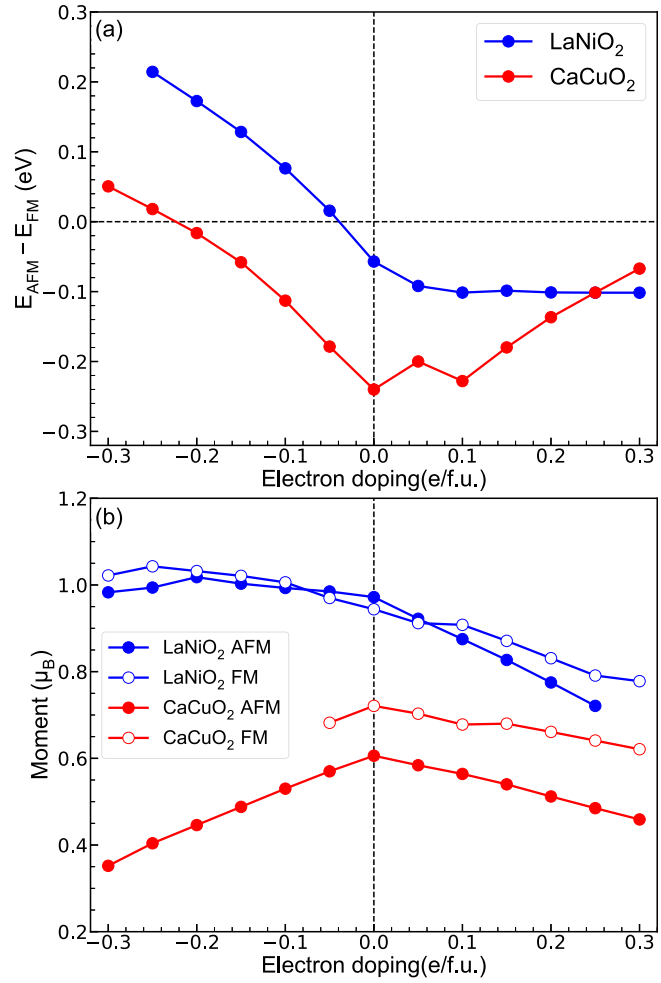

FIG. 7. HSE calculations of $LaNiO_2$ and $CaCuO_2$ at different doping concentrations. (a) The energy difference between G-type AFM and FM. (b) The local moment of Ni and Cu for G-type AFM and FM.

that resulted from small Δ_{dp} makes the d orbital difficult to be strongly polarized. In addition, due to the self-doping effect, the magnetic moments of cuprate and nickelate show completely different behaviors under doping. In nickelates, the additional electrons occupy the Nd-d orbitals; hence the moment tends to saturate gradually under electron doping. On the contrary, the moment in cuprate will decrease rapidly since there is no self-doping band and the O-p orbital will also suppress spin polarization especially in the FM state. The overall doping behavior of the energy difference between AFM and FM states as well as the moment are in great agreement with our DFT + U results and confirms our initial conclusions that Δ_{dp} and self-doping are the key factors responsible for the magnetic difference between the nickelates and the cuprates.

C. ED

In order to evaluate the exchange interaction's contribution to superconductivity, we further calculate the magnetic exchange interaction J between the Ni local magnetic moment in nickelate and compare it with cuprate. Based on the DFT and mean-field results above, if we simply map the total magnetic energy to the Heisenberg model to calculate the exchange interaction ($J \propto E_{\mathrm{AFM}} - E_{\mathrm{FM}}$), the calculated J will be close to zero because of the competition between the exchange interaction which favors AFM and the kinetic part which favors FM. Such an energy mapping method is applicable in undoped cuprates since the undoped cuprates are insulators. As for nickelates, the metallic behavior emerges because the itinerant holes are involved by self-doping bands, and then the kinetic energy contributes significantly to a total energy. Thus to obtain the exchange interaction in a metal, one must construct an equivalent substitution which can be treated as an insulator (see Ref. [33]) or include the kinetic term in calculations as an ED method. Now we follow the method in Refs. [26,42] and construct a three-band Hubbard model on Cu_5O_{16} and Ni_5O_{16} clusters. The parameters for Ni_5O_{16} are consistent with cuprate except with a smaller U_d^{Ni}=8 eV. To introduce the boundary interactions, we embed the clusters in an array of Cu/Ni-d^9 sites, which shifts the effective on-site energy of the outer O orbitals due to the intersite Coulomb energy. From the ED studies of half filled Cu_5O_{16} and Ni_5O_{16} clusters, we obtain the low-energy spectra with different Δ_{dp} values. These

spectra are matched with those of a nearest-neighbor spin-1/2 Heisenberg model ($H = \sum_{\langle ij \rangle} JS_iS_j$) with different exchange coupling J. As Fig. 3 shows, exchange coupling J is very sensitive to Δ_{dp}, but it is nearly not dependent on Coulomb interaction U_d. In the Cu_5O_{16} cluster, J is about 135 meV when $\Delta_{dp} = 3.6$ eV. While in the Ni_5O_{16} cluster, Δ_{dp} is 1.9 to 2.7 eV larger than Cu_5O_{16}, so that the exchange coupling J in Ni_5O_{16} cluster is about 62 ± 9 meV. Thus the effective AFM spin-spin interaction between the Ni local spin is not weak. The long-range magnetic order cannot be stabilized because of the large kinetic term, which can be treated as the t-J model.

D. DMFT calculation

Our DFT + U calculations indicate a larger local magnetic moment of Ni in $NdNiO_2$ than Cu in $CaCuO_2$ and a strong magnetic order in $NdNiO_2$. However, neutron diffraction experiments failed to observe sizable magnetic moments in the nickelates [8,15]. To explain this contradiction, we employ the DFT + DMFT method to investigate the dynamical screening processes of magnetic moment in nickelates.

To study the local moment of $NdNiO_2$ within DFT + DMFT, we compute the local spin-correlation functions $\chi(\tau) = \langle \hat{m}_z(\tau)\hat{m}_z(0)\rangle$. We first consider a Ni-d-only model as shown in Fig. 4(a); $\chi(0)$ of $d_{x^2-y^2}$ orbital without doping is about 0.9 μ_B^2. Upon 0.2 /f.u. hole doping, $\chi(0)$ is slightly reduced to 0.76 μ_B^2 and quickly decreases to 0.15 μ_B^2 when $\tau = \beta/2$ ($\tau = 19.34\,\text{eV}^{-1}$). The observed fast decay of χ at finite τ reflects a dynamical screening of the local moment due to spin fluctuations. The other orbitals, including t_{2g} and d_{z^2}, have no contributions to the magnetic moment.

To consider the Nd contribution, we then construct a Ni-d + Nd-d model with a total of 10 orbitals. As Fig. 4(b) shows, the instantaneous spin-correlation functions of the nominally undoped Ni-$d_{x^2-y^2}$ orbital are reduced to 0.8 μ_B^2 which is consistent with our previous DFT + U results. This size of moment indicates that the occupations in the Ni-$d_{x^2-y^2}$ orbital are slightly less than half filling. We see that when $\tau = \beta/2$, the spin-correlation functions of undoped Ni-$d_{x^2-y^2}$ orbital are screened to 0.24 μ_B^2, which is similar to the hole doped case in the d-only model. Meanwhile, other Ni-d orbitals have considerable instantaneous spin-correlation functions (~ 0.36 μ_B^2) and rapidly reduce to 0 for $\tau > 0$. The moment is further screened by doping which is the same with the Ni-d-only model. These phenomena indicate that the introduction of Nd-d orbitals plays a charge reservoir role, resulting in the decrease of occupations in Ni-$d_{x^2-y^2}$, leading to a smaller moment. When 0.2 /f.u. hole doping is applied, the spin-correlation functions of Ni-$d_{x^2-y^2}$ orbital are reduced to about 0.12 μ_B^2, and other orbitals exhibit the same behavior as the undoped case. The contribution of Nd-d orbitals is shown in the inset of Fig. 4(b). The instantaneous spin-correlation functions of undoped and 0.2 /f.u. hole doped Nd-d orbitals are 0.36 and 0.34 μ_B^2, respectively, and the spin-correlation functions of all these orbitals falls rapidly to 0 when τ increases. The difference between the Ni-d-only model and the Nd-d + Ni-d model is that the Ni-$d_{x^2-y^2}$ moment has been screened by Nd-d orbitals due to the self-doping effect without additional doping. DMFT benchmarks with density-density Hamiltonian give a similar consequence as discussed in Appendix D. Our DFT + DMFT calculations suggest that the self-doping effect in nickelates induces the screening effect to the Ni local moment; this reduces the time-average magnetic moment. In this respect, the frequency range of typical neutron experiments would be too limited to directly measure the magnitude of the moment of $NdNiO_2$.

We further investigate the temperature dependence of the magnetic moment of $NdNiO_2$ within the hole doping range from 0 to 0.2 /f.u. by studying a two-site Ni-d model. As Fig. 5 shows, without the inclusion of the Nd-d band, undoped $NdNiO_2$ has an AFM insulating ground state with

TABLE I. Energy comparison for Ni and Nd spin configurations with different U.

	U-Nd-f = 2.0 eV		U-Ni-d = 5.0 eV	
	Nd FM	Nd G-AFM	Nd C-AFM	Nd A-AFM
Ni FM	−0.059 eV	0.000 eV	−0.010 eV	−0.004 eV
Ni G-AFM	−0.053 eV	−0.046 eV	−0.052 eV	−0.049 eV
Ni C-AFM	−0.337 eV	−0.333 eV	−0.336 eV	−0.334 eV
Ni A-AFM	−0.062 eV	−0.052 eV	−0.059 eV	−0.056 eV
	U-Nd-f = 2.0 eV		U-Ni-d = 3.0 eV	
	Nd FM	Nd G-AFM	Nd C-AFM	Nd A-AFM
Ni FM	−0.348 eV	−0.387 eV	−0.397 eV	−0.391 eV
Ni G-AFM	−0.461 eV	0.000 eV	−0.359 eV	−0.393 eV
Ni C-AFM	−0.738 eV	−0.733 eV	−0.739 eV	−0.315 eV
Ni A-AFM	−0.445 eV	−0.435 eV	−0.443 eV	−0.332 eV
	U-Nd-f = 7.0 eV		U-Ni-d = 4.0 eV	
	Nd FM	Nd G-AFM	Nd C-AFM	Nd A-AFM
Ni FM	−0.297 eV	−0.147 eV	−0.400 eV	−0.149 eV
Ni G-AFM	−0.309 eV	−0.015 eV	−0.310 eV	−0.016 eV
Ni C-AFM	−0.344 eV	−0.355 eV	−0.290 eV	−0.356 eV
Ni A-AFM	−0.005 eV	−0.004 eV	−0.004 eV	0.000 eV

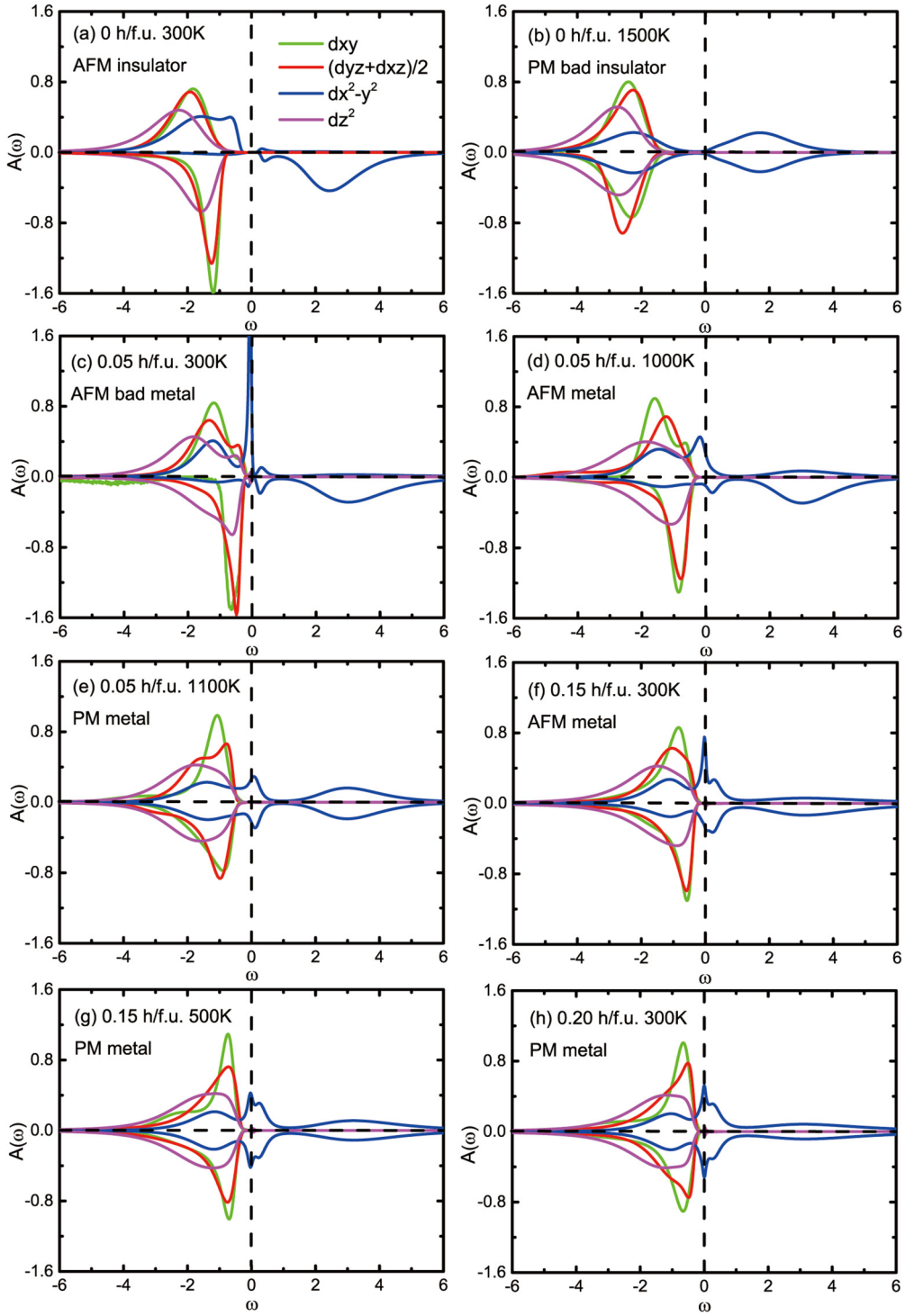

FIG. 8. Orbitally resolved spectral functions calculated by DFT + DMFT at different temperature and doping concentration. The positive and negative indicate spin-up and -down channels.

high Néel temperature, in stark contrast with experimental findings. This highlights the importance of the Nd-*d* band and its self-doping effect in determining the low-energy properties of the nickelates. We note that in addition to self-doping, several groups also emphasize the importance of hybridization between Nd-*d* and Ni-*d* [62,63,65]. Based on this and other earlier observations made in this work and the hybridization analysis in previous works [56,66,67], we thus emphasize that an appropriate minimal model of the nickelate should include the self-doping effect of Nd-*d*, thus clearly distinguishing the nickelate from the cuprate. In our work, the local moment is about 0.95 μ_B at low temperature, which decreases to zero when the temperature is above the Néel temperature. The Néel temperature is calculated to be about 1200 K, which is significantly higher than the experimental value due to the well-known DMFT overestimation of the magnetic transition

temperature of the AFM insulator by a factor of $2 \sim 3$ [68]. Upon hole doping, the local moment decreases gradually and drops to zero when the hole concentration reaches 0.2 /f.u. Meanwhile, the Néel temperature also decreases as the hole concentration increases. This evidence suggests that hole doping can suppress AFM coupling in $NdNiO_2$. By analyzing the orbital-resolved DMFT spectral function at different hole concentrations and temperatures (see Appendix D), we find that the insulator-metal transition also exists following the AFM-PM transition. For $NdNiO_2$ at 300 K without doping, the calculated spectral function shows that a gap is opened at the Fermi level, representing that the undoped $NdNiO_2$ is an AFM insulator at 300 K when the self-doping effect is excluded. The spectral function also indicates that $d_{x^2-y^2}$ orbital is nearly half filled, revealing its nature of the doped single-band Hubbard model [66]. When the temperature reaches 1500 K, the $d_{x^2-y^2}$ orbital has a nonzero contribution to the DOS near the Fermi energy, which is a sign of a bad insulator. The spectral function of $NdNiO_2$ at 300 K with 0.05 /f.u. hole doping shows that the band gap is closed and a finite peak appears at Fermi energy, indicating that the system is metallic but its conductivity is limited, i.e., a bad metal phase is obtained which is defined through the shape of electronic spectra $A(\omega)$ [69]. As the hole concentration or temperature continues to increase, $NdNiO_2$ finally becomes a metal.

IV. SUMMARY

In conclusion, we performed DFT + U, DMFT calculations and model analysis to investigate the magnetic properties of $NdNiO_2$ and $CaCuO_2$. We found that the magnetic properties of nickelates are significantly affected by both Δ_{dp} and doping. The large Δ_{dp} in $NdNiO_2$ results in a large local moment and spin splitting. It also decreases the AFM coupling. In addition, the self-doped holes frustrate the AFM. These effects together induce competing magnetic phase in nickelate, which differs from the dominating AFM phase in cuprate. Moreover, the mean-field calculations found that the ground state of 0.2 hole/f.u. doped $NdNiO_2$, which is in the superconduting state in experiment, is strikingly in an intralayer FM state. This may point to a phase with strong FM fluctuations in the highly doped nickelates, which may be explored in future experiments. The magnetic exchange interaction J estimated by ED of a small cluster is 62 ± 9 meV, comparable to (albeit quantitatively smaller than) that of the cuprates. This magnetic coupling should be quite important for understanding the physical mechanism of superconductivity in nickelates. In addition, the small magnetic moment observed in neutron-scattering experiments should be understood from a dynamical perspective. Other "faster" methods such as core-level spectroscopy may reveal a much larger local moment.

ACKNOWLEDGMENTS

We acknowledge financial support from the National Key R&D Program of China (Grants No. 2021YFA0718900, and No. 2017YFA0303602), the Key Research Program of Frontier Sciences of CAS (Grant No. ZDBS-LY-SLH008), the National Nature Science Foundation of China (Grants No. 11974365, No. 12004400, No. 11904373, and No. 51931011), the K.C. Wong Education Foundation (GJTD-2020-11), and the Ningbo Natural Science Foundation (202003N4363). Calculations were performed at the Supercomputing Center of Ningbo Institute of Materials Technology and Engineering and Vienna Scientific Clusters (VSC).

APPENDIX A: STRAIN EFFECT

To investigate the effect of substrate, we calculate the total energy and the local magnetic moment of $LaNiO_2$ and $CaCuO_2$ with a strain range from -3 to 3%. As Fig. 6 shows, the magnetic properties are not significantly influenced by strain, which suggests that the effect of substrate is negligible.

APPENDIX B: MAGNETIC ORDER

In the main text, we treat Nd-4f orbitals as core states and the magnetic moment of Nd is ignored for simplicity. Actually, the Nd-4f orbitals contribute a large moment and play an important role for further understanding the magnetic behavior of nickelates. As show in Table I, we calculate the magnetic order by including both magnetic moments of Ni and Nd, and the U dependent is also considered. All calculations indicate that the magnetic energy is mainly determined by the magnetic order of Ni.

APPENDIX C: HSE CALCULATION

In Fig. 2, we calculate magnetic moment and total energy at different doping concentrations with the DFT + U method. To verify the reliability of our conclusion, we have done the calculation with the HSE hybrid functional as shown in Fig. 7, which is consistent with DFT + U results. Therefore our conclusion is quite robust and will not be changed under a different functional.

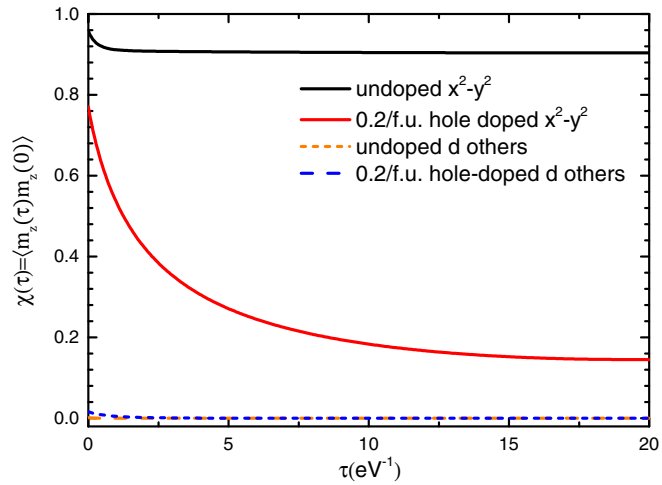

FIG. 9. Orbitally resolved local spin-correlation functions $\chi(\tau) = \langle \hat{m}_z(\tau)\hat{m}_z(0)\rangle$ calculated by DFT + DMFT at $T = 290$ K in the density-density form in d-only model, $\beta/2 \approx 20\ \mathrm{eV}^{-1}$.

APPENDIX D: DMFT CALCULATION

To show more details about the phase diagram of $NdNiO_2$ calculated by DMFT (see Fig. 5), especially for the definition of the conductivity (bad metal phase) and also the magnetic moment, we plot the spectral functions at different temperatures and hole doping concentrations in Fig. 8. As the orbital-resolved local spin-correlation functions (see Fig. 4) show in Sec. III D, the dynamical screening effect emerged in the Ni-*d* orbital. To compare with the Kanamori form in the main text, we also calculate the spin-correlation functions in density-density form as shown in Fig. 9, which is consist with the conclusions above.

[1] J. G. Bednorz and K. A. Müller, Z. Phys. B **64**, 189 (1986).
[2] C. Tsuei and J. Kirtley, Rev. Mod. Phys. **72**, 969 (2000).
[3] D. J. Scalapino, Rev. Mod. Phys. **84**, 1383 (2012).
[4] P. A. Lee, N. Nagaosa, and X.-G. Wen, Rev. Mod. Phys. **78**, 17 (2006).
[5] B. Keimer, S. A. Kivelson, M. R. Norman, S. Uchida, and J. Zaanen, Nature (London) **518**, 179 (2015).
[6] J. Zaanen, G. A. Sawatzky, and J. W. Allen, Phys. Rev. Lett. **55**, 418 (1985).
[7] F. C. Zhang and T. M. Rice, Phys. Rev. B **37**, 3759 (1988).
[8] M. Hayward, M. Green, M. Rosseinsky, and J. Sloan, J. Am. Chem. Soc. **121**, 8843 (1999).
[9] D. Li, K. Lee, B. Y. Wang, M. Osada, S. Crossley, H. R. Lee, Y. Cui, Y. Hikita, and H. Y. Hwang, Nature (London) **572**, 624 (2019).
[10] D. Li, B. Y. Wang, K. Lee, S. P. Harvey, M. Osada, B. H. Goodge, L. F. Kourkoutis, and H. Y. Hwang, Phys. Rev. Lett. **125**, 027001 (2020).
[11] S. Zeng, C.S. Tang, X. Yin, C. Li, M. Li, Z. Huang, J. Hu, W. Liu, G.J. Omar, H. Jani, Z.S. Lim, K. Han, D. Wan, P. Yang, S.J. Pennycook, A.T.S. Wee, and A. Ariando, Phys. Rev. Lett. **125**, 147003 (2020).
[12] Q. Gu, Y. Li, S. Wan, H. Li, W. Guo, H. Yang, Q. Li, X. Zhu, X. Pan, Y. Nie *et al.*, Nat. Commun. **11**, 6027 (2020).
[13] X. Zhou, X. Zhang, J. Yi, P. Qin, Z. Feng, P. Jiang, Z. Zhong, H. Yan, X. Wang, H. Chen *et al.*, Adv. Mater. **34**, 2106117 (2021).
[14] D. Vaknin, E. Caignol, P. K. Davies, J. E. Fischer, D. C. Johnston, and D. P. Goshorn, Phys. Rev. B **39**, 9122 (1989).
[15] M. Hayward and M. Rosseinsky, Solid State Sci. **5**, 839 (2003).
[16] V. I. Anisimov, D. Bukhvalov, and T. M. Rice, Phys. Rev. B **59**, 7901 (1999).
[17] K.-W. Lee and W. E. Pickett, Phys. Rev. B **70**, 165109 (2004).
[18] E. Been, W.-S. Lee, H. Y. Hwang, Y. Cui, J. Zaanen, T. Devereaux, B. Moritz, and C. Jia, Phys. Rev. X **11**, 011050 (2021).
[19] I. Leonov, S. L. Skornyakov, and S. Y. Savrasov, Phys. Rev. B **101**, 241108(R) (2020).
[20] A. S. Botana and M. R. Norman, Phys. Rev. X **10**, 011024 (2020).
[21] M.-Y. Choi, K.-W. Lee, and W. E. Pickett, Phys. Rev. B **101**, 020503(R) (2020).
[22] J. Kapeghian and A. S. Botana, Phys. Rev. B **102**, 205130 (2020).
[23] F. Lechermann, Phys. Rev. B **101**, 081110(R) (2020).
[24] L. Si, W. Xiao, J. Kaufmann, J. M. Tomczak, Y. Lu, Z. Zhong, and K. Held, Phys. Rev. Lett. **124**, 166402 (2020).
[25] Z. Liu, Z. Ren, W. Zhu, Z. Wang, and J. Yang, npj Quantum Mater. **5**, 31 (2020).
[26] H. Zhang, L. Jin, S. Wang, B. Xi, X. Shi, F. Ye, and J.-W. Mei, Phys. Rev. Research **2**, 013214 (2020).
[27] S. Ryee, H. Yoon, T. J. Kim, M. Y. Jeong, and M. J. Han, Phys. Rev. B **101**, 064513 (2020).
[28] Y. Cui, C. Li, Q. Li, X. Zhu, Z. Hu, Y.-f. Yang, J. Zhang, R. Yu, H.-H. Wen, and W. Yu, Chin. Phys. Lett. **38**, 067401 (2021).
[29] Y. Fu, L. Wang, H. Cheng, S. Pei, X. Zhou, J. Chen, S. Wang, R. Zhao, W. Jiang, C. Liu *et al.*, arXiv preprint arXiv:1911.03177 (2019)
[30] J.Q. Lin, P. VillarArribi, G. Fabbris, A.S. Botana, D. Meyers, H. Miao, Y. Shen, D.G. Mazzone, J. Feng, S.G. Chiuzbaian, A. Nag, A.C. Walters, M. Garcia-Fernandez, K.J. Zhou, J. Pelliciari, I. Jarrige, J.W. Freeland, J. Zhang, J.F. Mitchell, V. Bisogni, X. Liu, M.R. Norman, and M.P.M. Dean, Phys. Rev. Lett. **126**, 087001 (2021).
[31] H. Lu, M. Rossi, A. Nag, M. Osada, D. Li, K. Lee, B. Wang, M. Garcia-Fernandez, S. Agrestini, Z. Shen *et al.*, Science **373**, 213 (2021).
[32] V. M. Katukuri, N. A. Bogdanov, O. Weser, J. van den Brink, and A. Alavi, Phys. Rev. B **102**, 241112(R) (2020).
[33] Y. Nomura, T. Nomoto, M. Hirayama, and R. Arita, Phys. Rev. Research **2**, 043144 (2020).
[34] R. Ortiz, P. Puphal, M. Klett, F. Hotz, R. Kremer, H. Trepka, M. Hemmida, H.-A. K. von Nidda, M. Isobe, R. Khasanov *et al.*, Phys. Rev. Research **4**, 023093 (2022).
[35] S. Huangfu, Z. Guguchia, D. Cheptiakov, X. Zhang, H. Luetkens, D. J. Gawryluk, T. Shang, F. O. von Rohr, and A. Schilling, Phys. Rev. B **102**, 054423 (2020).
[36] G. Kresse and J. Furthmüller, Comput. Mater. Sci. **6**, 15 (1996).
[37] J. P. Perdew, K. Burke, and M. Ernzerhof, Phys. Rev. Lett. **77**, 3865 (1996).
[38] G. Kresse and J. Furthmüller, Phys. Rev. B **54**, 11169 (1996).
[39] P. Blaha, K. Schwarz, G. K. H. Madsen, D. Kvasnicka, J. Luitz, R. Laskowski, F. Tran, and L. D. Marks, *WIEN2k: An Augmented Plane Wave and Local Orbitals Program for Calculating Crystal Properties* (Vienna University of Technology, Austria, 2001).
[40] A. V. Krukau, O. A. Vydrov, A. F. Izmaylov, and G. E. Scuseria, J. Chem. Phys. **125**, 224106 (2006).
[41] J. Sun, A. Ruzsinszky, and J. P. Perdew, Phys. Rev. Lett. **115**, 036402 (2015).
[42] M. S. Hybertsen, E. B. Stechel, M. Schluter, and D. R. Jennison, Phys. Rev. B **41**, 11068 (1990).
[43] M. W. Haverkort, M. Zwierzycki, and O. K. Andersen, Phys. Rev. B **85**, 165113 (2012).
[44] G. H. Wannier, Phys. Rev. **52**, 191 (1937).
[45] N. Marzari, A. A. Mostofi, J. R. Yates, I. Souza, and D. Vanderbilt, Rev. Mod. Phys. **84**, 1419 (2012).
[46] A. A. Mostofi, J. R. Yates, Y.-S. Lee, I. Souza, D. Vanderbilt, and N. Marzari, Comput. Phys. Commun. **178**, 685 (2008).
[47] J. Kuneš, R. Arita, P. Wissgott, A. Toschi, H. Ikeda, and K. Held, Comput. Phys. Commun. **181**, 1888 (2010).

[48] T. Miyake and F. Aryasetiawan, Phys. Rev. B **77**, 085122 (2008).
[49] H. Sakakibara, H. Usui, K. Suzuki, T. Kotani, H. Aoki, and K. Kuroki, Phys. Rev. Lett. **125**, 077003 (2020).
[50] Y. Nomura, M. Hirayama, T. Tadano, Y. Yoshimoto, K. Nakamura, and R. Arita, Phys. Rev. B **100**, 205138 (2019).
[51] E. Gull, A. J. Millis, A. I. Lichtenstein, A. N. Rubtsov, M. Troyer, and P. Werner, Rev. Mod. Phys. **83**, 349 (2011).
[52] N. Parragh, A. Toschi, K. Held, and G. Sangiovanni, Phys. Rev. B **86**, 155158 (2012).
[53] M. Wallerberger, A. Hausoel, P. Gunacker, A. Kowalski, N. Parragh, F. Goth, K. Held, and G. Sangiovanni, Comput. Phys. Commun. **235**, 388 (2019).
[54] J. E. Gubernatis, M. Jarrell, R. N. Silver, and D. S. Sivia, Phys. Rev. B **44**, 6011 (1991).
[55] A. W. Sandvik, Phys. Rev. B **57**, 10287 (1998).
[56] P. Jiang, L. Si, Z. Liao, and Z. Zhong, Phys. Rev. B **100**, 201106(R) (2019).
[57] P. Hansmann, N. Parragh, A. Toschi, G. Sangiovanni, and K. Held, New J. Phys. **16**, 033009 (2014).
[58] T. Sarkar, D. Wei, J. Zhang, N. Poniatowski, P. Mandal, A. Kapitulnik, and R. L. Greene, Science **368**, 532 (2020).
[59] J. Sonier, C. Kaiser, V. Pacradouni, S. Sabok-Sayr, C. Cochrane, D. MacLaughlin, S. Komiya, and N. Hussey, Proc. Natl. Acad. Sci. USA **107**, 17131 (2010).
[60] F. Deng, P. Jiang, Y. Lu, and Z. Zhong, EPL (Europhys. Lett.) **135**, 67001 (2021).
[61] A. Chiciak, E. Vitali, H. Shi, and S. Zhang, Phys. Rev. B **97**, 235127 (2018).
[62] Y. Gu, S. Zhu, X. Wang, J. Hu, and H. Chen, Commun. Phys. **3**, 84 (2020).
[63] Y.-f. Yang and G.-M. Zhang, Frontiers in Physics **9**, 801236 (2022).
[64] M. J. Rozenberg, G. Kotliar, H. Kajueter, G. A. Thomas, D. H. Rapkine, J. M. Honig, and P. Metcalf, Phys. Rev. Lett. **75**, 105 (1995).
[65] G.-M. Zhang, Y.-f. Yang, and F.-C. Zhang, Phys. Rev. B **101**, 020501(R) (2020).
[66] M. Kitatani, L. Si, O. Janson, R. Arita, Z. Zhong, and K. Held, npj Quantum Mater. **5**, 59 (2020).
[67] J. Karp, A. S. Botana, M. R. Norman, H. Park, M. Zingl, and A. Millis, Phys. Rev. X **10**, 021061 (2020).
[68] A. I. Lichtenstein, M. I. Katsnelson, and G. Kotliar, Phys. Rev. Lett. **87**, 067205 (2001).
[69] G. Kotliar and D. Vollhardt, Phys. Today **57**, 3, 53 (2004).